lar organ, and has been suggested to be particularly susceptible to parenchymal bleeding when the architecture is damaged by disease, trauma or vascular obstruction and infection, notably in settings of coexistent coagulation disorder. Factors that might explain pathological splenic rupture in hematological malignancies include: (1) infiltration into the spleen of tumor cells changing the histological structure of the spleen; (2) splenic infarction inducing severe structural weakness, and (3) local coagulation disorders leading to intrasplenic and subcapsular bleeding, ultimately resulting in capsular rupture [17]. Coagulation disturbance or thrombocytopenia may play major roles in the pathogenesis of splenic rupture. However, correlations between splenic rupture and coagulation disturbances have not yet been confirmed in any cases. In addition, thrombocytopenia does not seem to increase the risk of splenic rupture. A review by Bauer et al. [17] found no significant correlation between survival and platelet number, leukocyte count, or size of the spleen.

In normal Japanese 50- to 54-year-old females, the mean weight of the spleen is 83.3 ± 34.0 g [18]. The spleen is enclosed within the capsule. In the present case, the spleen weighed 1,236 g at autopsy. Even if the spleen undergoes a considerable increase in size, this internal organ does not rupture easily. Autopsy in the present case revealed ATL cells diffusely infiltrating throughout the spleen and penetrating the capsule. In addition, the capsule of the spleen was stretched and thin due to splenomegaly. However, no splenic infarction or intrasplenic or subcapsular bleeding was identified. These results strongly suggest that thinning of the capsule due to rapid splenomegaly and direct infiltration of ATL cells penetrating the capsule caused splenic rupture in the present case.

Emergency splenectomy represents the only feasible treatment for splenic rupture. Among 136 cases of pathological splenic rupture reported in the literature, 88 patients underwent surgical intervention, while 43 patients were managed without operation. No information could be obtained for the 5 remaining cases. Of the 88 patients who underwent surgical intervention, 55 (63%) survived and 33 (37%) died. Of the 43 patients who did not undergo surgery, 40 died [3]. Splenic surgery in patients with hematological malignancy carries a high mortality and morbidity, due to an increased risk of hemorrhage and infection. In patients with hematological malignancy, pathological rupture of the spleen often happens unexpectedly, with no preceding trauma. Diagnosis is therefore often difficult. The present case displayed a sudden decrease in blood pressure, but no abdominal pain. Careful observation, particularly at the end stage accompanying rapid tumor growth, is therefore necessary when splenic rupture is deemed possible. Using ultrasonography or computer tomography, peritoneal aspiration of fresh blood may assist in the diagnosis of pathological splenic rupture. When the diagnosis is made, emergency splenectomy should be performed.

References

1 Lieberman ME, Levitt A: Spontaneous rupture of the spleen: A case report and literature review. Am J Emerg Med 1989;7:28–31.
2 Schiødt I, Duun E, Fischer TK, Christiansen AP, Ralfkiaer E: Fatal rupture of the spleen caused by infiltration of T-cell lymphoma. Ann Hematol 2000;79:158–160.
3 Giagounidis AAN, Burk M, Meckenstock G, Koch AJ, Schneider W: Pathologic rupture of the spleen in hematologic malignancies: Two additional cases. Ann Hematol 1996;73:297–302.
4 Knoblich R: Pathologic (so-called spontaneous) rupture of spleen in leukaemia and lymphoma. Mich Med 1966;65:105–114.
5 Papesch M, Watkins R: Epstein-Barr virus infectious mononucleosis. Clin Otolaryngol 2001;26:3–8.
6 Zingman BS, Viner BL: Splenic complications in malaria: Case report and review. Clin Infect Dis 1993;16:223–232.
7 Shimoyama M: Diagnostic criteria and classification of clinical subtypes of adult T-cell leukaemia-lymphoma. A report from the Lymphoma Study Group (1984–1987). Br J Haematol 1991;79:428–437.
8 Tobinai K: Chemotherapy: the more, the better in malignant lymphoma? Cancer Chemother Pharmacol 1997;40:110–114.
9 Hyun BH, Varga CF, Rubin RJ: Spontaneous and pathologic rupture of the spleen. Arch Surg 1977;104:652–657.
10 Lam KY, Ng WF, Chan AC: Miliary tuberculosis with splenic rupture: A fatal case with hemophagocytic syndrome and possible association with long standing sarcoidosis. Pathology 1994;26:493–496.
11 Fishman D, Isenberg DA: Splenic involvement in rheumatic diseases. Semin Arthritis Rheum 1997;27:141–155.
12 Karassa FB, Isenberg DA: Spontaneous rupture of the spleen: An unusual complication of systemic lupus erythematosus. Lupus 2001;10:876–878.
13 Oran B, Wright DG, Seldin DC, McAneny D, Skinner M, Sanchorawala V: Spontaneous rupture of the spleen in AL amyloidosis. Am J Hematol 2003;74:131–135.
14 Shimamoto Y, Yamaguchi M: HTLV-I induced extranodal lymphomas. Leuk Lymphoma 1992;7:37–45.
15 Bennett SR, Greer JP, Stein RS, Glick AD, Cousar JB, Collins RD: Death due to splenic rupture in suppressor cell mycosis fungoides: A case report. Am J Clin Pathol 1984;82:104–109.
16 Debnath D, Valerio D: Atraumatic rupture of the spleen in adults. R Coll Surg Edinb 2002;47:437–445.
17 Bauer TW, Haskins GE, Armitage JO: Splenic rupture in patients with hematologic malignancies. Cancer 1981;48:2729–2733.
18 Ogiu N, Nakamura Y, Ijiri I, Hiraiwa K, Ogiu T: A statistical analysis of the internal organ weights of normal Japanese people. Health Phys 1997;72:368–383.

Journal of Neurochemistry, 2005, **92**, 759–766 doi:10.1111/j.1471-4159.2004.02924.x

A gene-targeted mouse model for chorea-acanthocytosis

Yuko Tomemori,* Mio Ichiba,* Akira Kusumoto,* Emiko Mizuno,* Daisuke Sato,* Shinji Muroya,* Masayuki Nakamura,* Hiroaki Kawaguchi,† Hiroki Yoshida,† Shu-ichi Ueno,‡ Kazuki Nakao,§ Kenji Nakamura,¶ Atsu Aiba,** Motoya Katsuki†† and Akira Sano*

*Departments of *Psychiatry and †Pathology, Kagoshima University Graduate School of Medical and Dental Sciences, Kagoshima, Japan*

‡Department of Psychiatry, Course of Integrated Brain Sciences, University of Tokushima School of Medicine, Tokushima, Japan

§Laboratory for Animal Resources and Genetic Engineering, Riken Center for Developmental Biology, Kobe, Japan

¶Reproductive Engineering Section, Mitsubishi Kagaku Institute of Life Sciences, Tokyo, Japan

***Division of Cell Biology, Department of Molecular and Cellular Biology, Kobe University Graduate School of Medicine, Kobe, Japan*

††National Institute for Basic Biology, Okazaki, Japan

Abstract

Chorea-acanthocytosis (CHAC) is a hereditary neurodegenerative disorder with autosomal recessive transmission, in which selective degeneration of striatum has been reported in brain pathology. Clinically, CHAC shows Huntington's disease-like neuropsychiatric symptoms and red blood cell acanthocytosis. Recently, we identified the gene, *CHAC*, encoding a novel protein, chorein, in which a deletion mutation was found in Japanese families with CHAC. In the present study, we have identified the mouse *CHAC* cDNA sequence and the exon–intron structures of the gene and produced a CHAC model mouse introducing no. 60–61 exon deletion corresponding to a human disease mutation by a gene-targeting technique. The mice began to show acanthocytosis and motor disturbance in old age. In behavioral observations, locomotor activity was significantly decreased and the contact time at social interaction test was decreased significantly in the model mice. In the brain pathology, many apoptotic cells were observed in the striatum of the mutant mice. In neurochemical determinations, the dopamine metabolite, homovanillic acid, concentration decreased significantly in the portion including the midbrain of the mutant mice. These findings are consistent with the human results reported elsewhere and indicate that the CHAC model mice showed a mild phenotype with late adult onset. The CHAC model mouse therefore provides a good model system to study the human disease.

Keywords: *CHAC*, chorea-acanthocytosis, chorein, gene-targeted mouse model, neurodegeneration.

J. Neurochem. (2005) **92**, 759–766.

Chorea-acanthocytosis (CHAC; MIM 200150) is a rare autosomal recessive neurodegenerative disorder, relatively more frequent in Japan (Rampoldi *et al.* 2002). Clinically, CHAC is best characterized by the gradual and adult onset of chorea and acanthocytosis in erythrocytes. In addition, other neuropsychiatric deficits, such as oral dyskinesia and dystonia frequently with self-mutilation, personality change, schizophrenia-like symptoms, dementia, myopathy and peripheral neuropathy, often take place (Brin 1993). Dilated cardiomyopathy has been reported in some patients with CHAC (Kageyama *et al.* 2000). The main neuropathological finding of CHAC is the degeneration of striatum (Hardie *et al.* 1991).

Recently, we and others identified the gene *CHAC* that is responsible for CHAC (Rampoldi *et al.* 2001; Ueno *et al.* 2001). The *CHAC* gene exists on human chromosome 9q21 spanning a 250-kb region and consists of 73 exons. Although

Received August 13, 2004; revised manuscript received October 1, 2004; accepted October 3, 2004.

Address correspondence and reprint requests to Akira Sano, MD, PhD, Department of Psychiatry, Kagoshima University Graduate School of Medical and Dental Sciences 8-35-1 Sakuragaoka, Kagoshima 890-8520, Japan. E-mail: sano@m3.kufm.kagoshima-u.ac.jp

Abbreviations used: CHAC, chorea-acanthocytosis; HVA, homovanillic acid; TUNEL, terminal transferase biotinylated-UTP nick end-labeling.

the function of chorein, the product of *CHAC*, is unclear, the homologs have been found in *Saccharomyces cerevisiae* and *Dictyosteium discoideum* (Brickner *et al.* 1997). The null mutant of the *S. cerevisiae* homolog *VPS13* is viable but shows defects in vacuolar protein sorting and a *TipC* gene mutant of *D. discoideum* has aberrant cell-sorting behavior so chorein is thought to play a role in the dynamic change of cellular structures.

Chorea-acanthocytosis is very rare and the number of autopsied cases is limited, so it is difficult to study the molecular pathogenesis of CHAC using human specimens. Therefore, the CHAC model mouse is very valuable. Here we report the production and characterization of a *CHAC* mutant mouse which carries a CHAC-causative Ehime deletion mutation found in Japanese patients with CHAC (Ueno *et al.* 2001).

Materials and methods

Search for mouse homolog of chorea-acanthocytosis gene

To identify the mouse homolog of *CHAC*, we searched the expressed sequence tags (ESTs) on the NCBI database. RT-PCR was carried out with primer setting according to reported mouse EST sequences. Total RNA, for use as RT-PCR template, was extracted from C57BL/6J mouse leukocytes using the QIAamp RNA Blood Mini Kit (Qiagen, Valencia, CA, USA). For detection of the 5′ and 3′ ends, we conducted 5′ RACE (rapid amplification of cDNA ends) and 3′ RACE using the SMART RACE cDNA Amplification Kit (CLONTECH, Palo Alto, CA, USA). Direct sequencing was carried out after RT-PCR.

Generation of the chorea-acanthocytosis deletion mice

We screened a library prepared from 129/Sv mouse genomic DNA (RP22; Invitrogen, Carlsbad, CA, USA) with the use of mouse *CHAC* cDNA. For the construction of the targeting vector of the *CHAC* gene, we subcloned a *PmaCI-SpeI* 8.9-kb genomic DNA fragment. An internal 3.7-kb *ApaI-SalI* fragment including exons 60 and 61, which is deleted in the human CHAC-liable Ehime deletion mutation, was replaced with the neomycin resistance gene. A 1.1-kb diphtheria toxin gene fragment was attached to the 3′ end of the targeting vector for negative selection (Yagi *et al.* 1993). Electroporation of the targeting vector into embryonic stem cells (CCE, 129/Sv background), selection of embryonic stem cells containing the properly targeted gene, generation of 129/Sv/C57BL/6J chimeric mice and germline transmission for the generation of heterozygous mutant F_1 mice in a 129/Sv/C57BL/6J background were carried out as previously described (Koera *et al.* 1997). A typing PCR of the *CHAC* genes was carried out using tail DNA as the template and

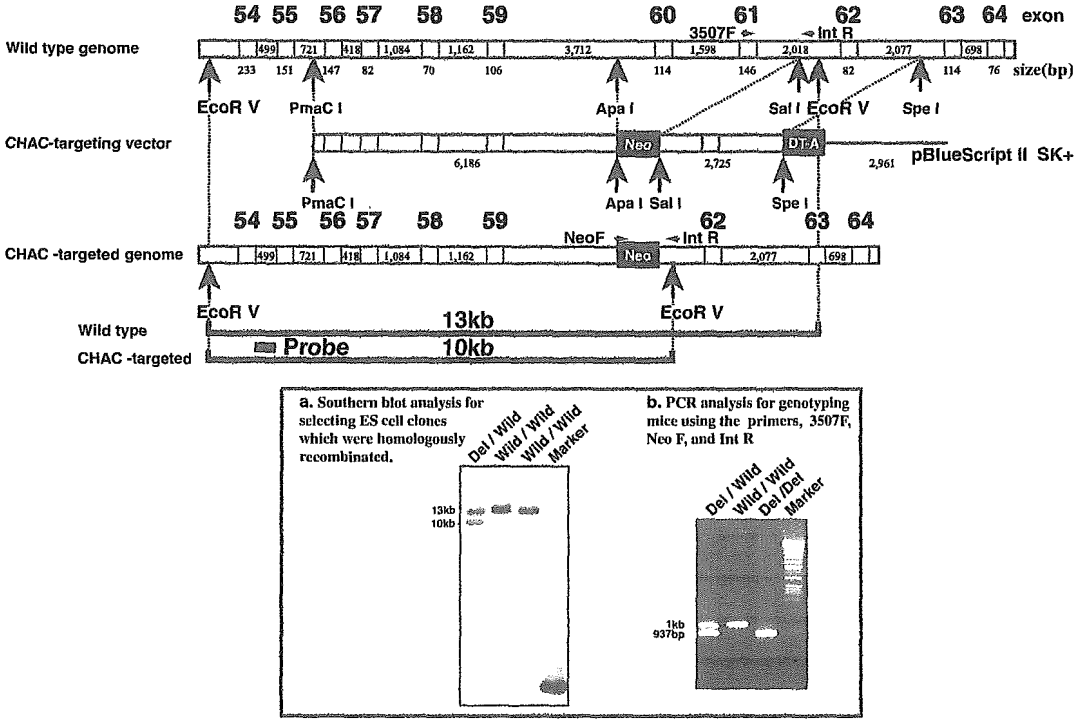

Fig. 1 *Targeted disruption of the CHAC gene.* Homologous recombination resulted in replacement of the 3.7-kb fragment including exons 60 and 61 with the neomycin resistance gene (Neo). The diphtheria toxin gene (DT-A) was attached to the 3′ end of the targeting vector for negative selection. Restriction sites are indicated by arrows. The location of the probe used for Southern blot analysis is indicated. *Eco*RV-digested DNAs were hybridized with the probes. The results of Southern blot analysis for selecting embryonic stem (ES) cell clones and PCR analysis for genotyping mice are shown in the inset.

primers illustrated in Fig. 1. We observed closely and checked body weight once a week. The use of animals in this research complied with all relevant guidelines of the Japanese government, Institute of Medical Science, University of Tokyo and Kagoshima University.

Osmotic fragility test of red blood cells

Blood was extracted by cutting the axillary vein and collecting in a syringe with heparin to avoid blood coagulation. Each 20 μL was dropped into a gradient concentration of phosphate-buffered NaCl solution (0.85, 0.75, 0.70, 0.65, 0.60, 0.55, 0.50, 0.45, 0.40, 0.35, 0.30, 0.20 and 0.10%, respectively). The hemolytic ratio was calculated by determining the absorbance at 540 nm and the concentration of NaCl (%) to cause 50% hemolysis (C_{50}) was estimated (Try 1980). Results (mean ± SD of seven mutant and nine wild-type mice) are expressed as C50 ± SD.

Footprint pattern

The footprint pattern was used to compare the gait of *CHAC* mutant mice with that of wild-type control mice (Carter *et al.* 1999). To obtain footprints, the hind- and forefeet of the mice were coated with red and green non-toxic paints, respectively. The animals were then allowed to walk along a 50 cm long, 10 cm wide runway (with 10 cm high walls) into an enclosed box. A fresh sheet of white paper was placed on the floor of the runway for each run. Stride length was measured as the average distance of forward movement between each stride. The mean value of each set of three values was used in subsequent analysis ($n = 13$, homozygous mutant mice and $n = 20$, wild-type mice).

Rotarod

The rotarod apparatus (Rotarod; O'Hara & Co., Ltd, Tokyo, Japan) was used to measure fore- and hindlimb motor coordination and balance. Rotarod training consisted of placing the animals on the rotating rod at a speed of 24 r.p.m. for 1 min. Mice received four trials per day for three consecutive days, by which time a steady baseline level of performance was attained (Carter *et al.* 1999). Mice then received two trials at 10 increasing speeds from 15 r.p.m. The mean latency to fall off the rotarod was recorded and used in a subsequent analysis ($n = 13$, homozygous mutant mice and $n = 20$, wild-type mice).

Open field analysis

Animals were put off the rack for 1 h before the test to accustom them to the novel environment and then placed in a box (50 × 50 cm). Traces were drawn for 10 min by an image-analysing program (Image OF4; O'hara & Co., Ltd) and the total moving distance was calculated ($n = 13$, homozygous mutant mice and $n = 20$, wild-type mice).

Social behavior

We conducted a social interaction test between two male mice of the same genotype group. Each group consisted of eight samples. Mice were reared with one to four other mice per cage. After accustoming the mice as described for open field analysis, two mice were placed in a closed 50 × 50 cm box and traces were drawn by the image-analysing programs Image OFC and SI (O'hara & Co., Ltd). The test lasted for 2 min per session and the total moving distances of the mice and contact time were calculated.

Monoamine and amino acid analysis

Brains were removed from *CHAC* mice homozygous for the transgene ($n = 6$) and normal littermate ($n = 6$) controls at 79–84 weeks of age and dissected on ice basically according to the method of Glowinski and Iversen (McIlwain and Voaden 1975). Tissues were stored frozen at −80°C until analysis for neurotransmitter content. Levels of the monoamine neurotransmitters and metabolites were determined separately by established HPLC methods using electrochemical detection (Reynolds and Pearson 1987). GABA was analysed using the same samples by HPLC coupled to post-column ninhydrin derivatization with spectrophotometry.

Histological analysis

Four homozygous mutant and five wild-type mice (72–84-week-old females) were deeply anesthetized with sodium pentobarbital and perfused through the left ventricle with cold 4% paraformaldehyde in 0.1 M sodium phosphate buffer at pH 7.4. Brain and other organs were removed and post-fixed in the respective perfusion solution overnight at 4°C. The tissues were dehydrated and embedded in paraffin. For immunohistochemistry coronal sections of the brain were cut on a microtome at 4 μm. Tissue sections were deparaffinized and rehydrated after cutting samples. All brain sections were incubated with methanol containing 0.3% H_2O_2 to block endogenous peroxidase activity and then incubated with a primary antiserum diluted with 0.05 M Tris-buffered saline containing 0.2% Triton X-100 for glial fibrillary acidic protein (1/500; rabbit polyclonal; Dako, Glostrup, Denmark) overnight at 4°C. Immunoreactive products were detected using a Vectastatin ABC Kit (Vector Laboratories, Burlingame, CA, USA) and then visualized after adding DAB (3,3′-Diamino-benzidine tetrohydrochloride) as the chromogen. For Terminal transferase biotinylated-UTP nick end-labeling (TUNEL) stain, we used the Fast Red Substrate System (Dako). Tissue sections were counterstained with hematoxylin. TUNEL-positive cells were counted in five fields on one side of the striatum in six mice (three wild-type and three mutant mice). The number of positive cells was examined by statistical analysis.

Statistical analysis

All statistical analyses were performed using Mann–Whitney's *U*-test for comparisons between wild-type and *CHAC* mutant. All data are presented as mean ± SD.

Results

Cloning of mouse chorea-acanthocytosis homolog

To obtain the mouse homolog of the human *CHAC* gene, various combinations of primers generated from the sequence of the human *CHAC* gene (Ueno *et al.* 2001) were tested using RT-PCR. Some primer sets gave rise to suitable products using cDNA from mouse brain as template. We extended the assembled sequence to both 5′ and 3′ directions by the RACE method. The total number of sequenced nucleotides was 9861 bp (Accession no. DDBJ AB115421).

The ATG at nucleotide residues 160–162 is likely to be the translation initiation codon and an in-frame TGA stop codon is present at nucleotide residues 9658–9660, which suggests that it codes for a protein of 3166 amino acids. The cDNA sequence was compared with the reported mouse genomic sequence (Accession no. NT_039687) and 72 exons with proper consensus exon–intron boundary sequences were confirmed in the genomic sequence.

Gene targeting of chorea-acanthocytosis

In order to produce a CHAC model mouse by introducing the no. 60–61 exon deletion corresponding to a human disease mutation (Ueno *et al.* 2001), we first isolated an 8.9-kb fragment containing mouse *CHAC* exons 60 and 61 from the 129/Sv genomic BAC library. We assembled a targeting vector to replace from the middle of intron 59 to the middle of intron 61 by a neomycin resistance cassette (Fig. 1). The successful deletion was confirmed at genome level by Southern blot (Fig. 1 inset). The consequence of such aberrant splicing in this putative coding mRNA is the change of the open reading frame (ORF) from position codon 2730 and the appearance of a stop codon at position 2735. Germline transmission was obtained with chimeric mice. F_1 and F_2 mice were confirmed by PCR (Fig. 1 inset). Mice carrying the homozygous mutation were viable. We obtained 101 offspring by *CHAC* deletion F_1 heterozygote matings. The genotypes were 20.8% (21/101) homozygous mutant, 35.6% (36/101) wild-type and 43.6% (44/101) heterozygous mutant. There was no segregation distortion between genotypes and no significant difference in survival ratio (Fig. 2) and body weight at the age of 87 weeks. Involuntary movements were not found. Mice with the genotype del/del were used as *CHAC* mutant mice for the experiments below together with wild-type controls.

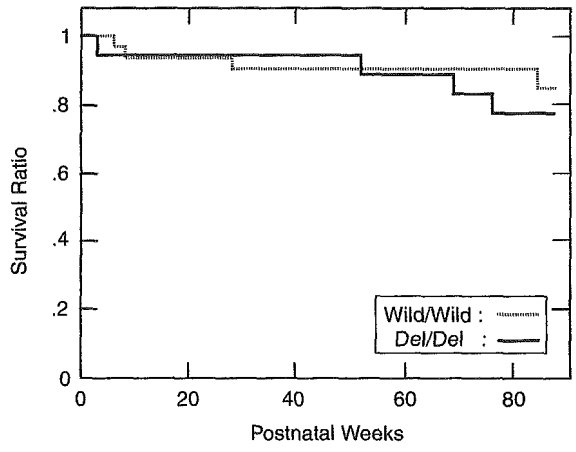

Fig. 2 Survival curve. We obtained 101 F_2 mice consisting of 21 homozygous mutant, 44 heterozygous mutant and 36 wild-type mice. There was no significant difference in survival ratio between wild-type and homozygous mutant mice at the end of observation.

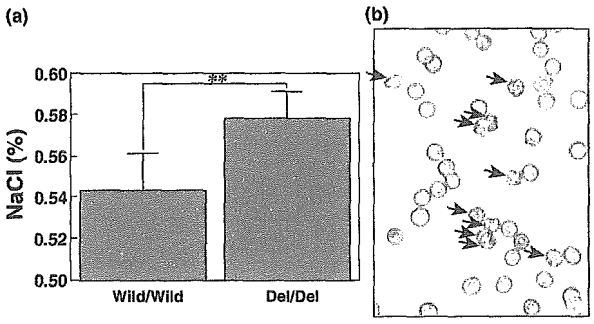

Fig. 3 (a) Osmotic fragility test of red blood cells. Each 20 μL of blood from wild-type and homozygous *CHAC* mutant mice was mixed with 2 mL of phosphate-buffered NaCl solutions with concentrations of 0.85, 0.75, 0.70, 0.65, 0.60, 0.55, 0.50, 0.45, 0.40, 0.35, 0.30, 0.20 and 0.10%, respectively. The hemolytic ratio was calculated by determining the absorbance at 540 nm and the concentration of NaCl (%) to cause 50% hemolysis (C50) was estimated. Results (mean ± SD of 13 mutant and 20 wild-type mice) are expressed as C50 ± SD. Significant difference between wild-type control and *CHAC* mutant mice (**$p < 0.01$). (b) Many acanthocytes indicated by arrows were observed in peripheral blood smears of *CHAC* mutant mice.

Hematological analysis

Light microscopy of red blood cells

Light microscopic observation of peripheral blood smears of *CHAC* mutant mice showed heterogeneity in sizes and shapes of the erythrocytes, including acanthocytes (Fig. 3b).

Osmotic fragility analysis of red blood cells

The osmotic fragility test is the most sensitive test available to detect cells that are less tolerant to osmotic stress than normal cells (Becker and Lux 1995). The red blood cells from *CHAC* mutant mice showed an increase in their *in vitro* osmotic fragility when exposed to hypotonic NaCl solutions. We found that the NaCl concentration that produced 50% hemolysis (C50) was significantly higher in the mutant mice (Fig. 3b). C50 values were 0.578% (w/v) NaCl for *CHAC* mutant mice and 0.543% NaCl for wild-type mice. A marked increase in the osmotic fragility of red blood cells in the *CHAC* mutant mice together with acanthocytosis defines a full set of hematological abnormal findings seen in human CHAC (Palek 1991).

Motor function

Footprint test

Gait disturbance was assessed by analysing the footprint patterns while mice walked along a narrow corridor. Footprint patterns of wild-type and *CHAC* mutant mice at 84–87 weeks of age were illustrated. Wild-type mice walked in a straight line with a regular even alternating gait, placing the hindpaw precisely at the position where the ipsilateral

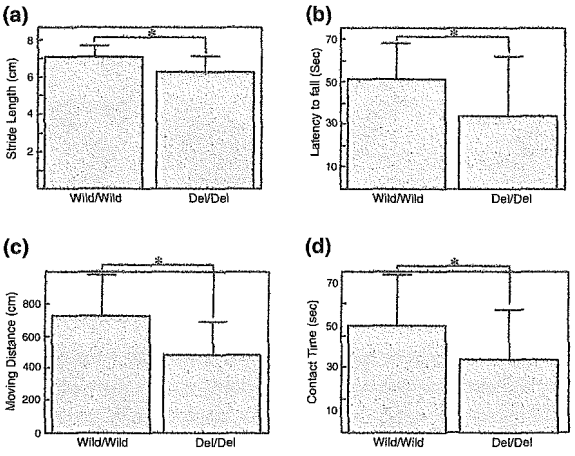

Fig. 4 (a) Quantitative analysis of stride length. Walking footprint patterns were produced by wild-type and *CHAC* mutant mice and stride lengths were then determined. The average stride length of the *CHAC* mutant mice was significantly less than that of wild-type mice (*$p < 0.05$). (b) Balance and motor coordination on the rotarod. Wild-type ($n = 20$) and *CHAC* mutant ($n = 13$) mice were subjected to an accelerating rotarod. The means ± SD of the latency to fall (maximum trial duration, 60 s) for each two trials were recorded. The *CHAC* mutant mice exhibited poorer performance on rotarod than wild-type mice. Significant difference between wild-type control and *CHAC* mutant mice (*$p < 0.05$). (c) Open field analysis. Basal motor activity in control wild-type and *CHAC* mutant mice at 70–82 weeks of age. Locomotor activity measured by moving distance was decreased in the *CHAC* mutant mice (*$p < 0.05$). (d) Social interaction analysis. Each two mice were placed in a closed 50 × 50 cm box and traces drawn by image-analysing programs. The tests lasted for 2 min per session. Total moving distances of the mice and contact time were calculated. Total contact time was significantly decreased in the *CHAC* mutant mice (*$p < 0.05$).

forepaw had been in the previous step. By contrast, *CHAC* mutant mice walked with short steps and their hindpaws were not on the forepaws. The resulting footprint patterns were assessed quantitatively by measuring the stride length. The mean stride length of *CHAC* mutant mice was significantly shorter compared with that of control mice (Fig. 4a, $p < 0.05$).

Rotarod test

Motor coordination and balance of the mice were measured using a rotarod. The mean latency to fall off was significantly shorter in *CHAC* mutant compared with wild-type mice (Fig. 4b, $p < 0.05$). The broad range of SDs showed the existence of differences between individuals.

Locomotor activity and social interaction

Spontaneous locomotor activities in the open field were measured for 10 min in daytime with a behavioral tracing analyser (O'hara & Co., Ltd). The total moving distance in a

Table 1 Monoamines, their metabolites and GABA concentration in brain regions

	Cerebral cortex		Striatum		Hippocampus		Thalamus, hypothalamus midbrain		Cerebellum		Lower brainstem	
	Wild/wild	Del/del	Wild/wild	Del/del	Wild/wild	Del/del	Wild/wild	Del/del	Wild/wild	Del/del	Wild/wild	Del/del
Norepinephrine	215 ± 44	256 ± 26	86 ± 17	89 ± 7	336 ± 36	352 ± 63	461 ± 126	434 ± 60	182 ± 23	200 ± 50	451 ± 68	483 ± 90
Dopamine	402 ± 83	339 ± 144	10 864 ± 1975	9943 ± 1144	14 ± 4	13 ± 2	454 ± 113	350 ± 114	5 ± 1	5 ± 2	27 ± 7	27 ± 5
HVA	149 ± 11	158 ± 22	1082 ± 146	1095 ± 87	48 ± 8	52 ± 7	193 ± 22	160 ± 22*	48 ± 8	40 ± 18	44 ± 7	57 ± 20
5-HT	454 ± 87	384 ± 72	524 ± 145	413 ± 63	536 ± 69	465 ± 35	620 ± 170	611 ± 119	69 ± 33	65 ± 29	410 ± 113	393 ± 126
5-HIAA	325 ± 41	291 ± 12	394 ± 110	366 ± 44	441 ± 67	439 ± 74	763 ± 176	666 ± 61	151 ± 32	138 ± 36	540 ± 82	529 ± 57
GABA	ND	ND	1323 ± 174	1341 ± 316	ND	ND	2605 ± 525	2323 ± 240	ND	ND	ND	ND

Data are mean ± SD values, in ng/g of tissue, from six animals per group. 5-HIAA, 5-hydroxyindoleacetic acid; 5-HT, 5-hydroxytryptamine; HVA, homovanillic acid.
*$p < 0.05$ vs. Wild/Wild.

novel environment in wild-type ($n = 20$) and *CHAC* mutant mice ($n = 13$) showed a significant difference (Fig. 4c, $p < 0.05$). Wild-type mice showed a tendency to spend more time in the center area (data not shown).

In the social interaction test, *CHAC* mutant mice showed less contact time (Fig. 4d, $p < 0.05$) and stayed in the edge area of the field for a significantly longer time.

Atrophy and neurotransmitter analysis in the brain

The weight ratio of one portion : whole brain was measured and we found a significant difference in the striatum. The ratio in *CHAC* mutant mice brain was smaller than that in wild-type mice ($p < 0.05$). Monoamines, their metabolites and GABA were measured from the homogenate of brain sections divided into six portions, hippocampus, striatum, cerebral cortex, cerebellar, brainstem and others (midbrain, thalamus and hypothalamus). Mean values of the dopamine level were less in *CHAC* mutant compared with wild-type mice in both striatum and the portion including midbrain but were not significant (9943 ± 1.144 vs. 10 864 ± 1975 ng/g, $p = 0.346$; 350 ± 114 vs. 454 ± 113 ng/g, $p = 0.142$, respectively). However, the level of the dopamine metabolite homovanillic acid (HVA) in the portion including midbrain was significantly less in the mutant mice (Table 1, $p < 0.05$). Such a mild and insignificant decrease was observed in the level of GABA in the portion including midbrain (2323 ± 240 vs. 2605 ± 525 ng/g; $p = 0.262$).

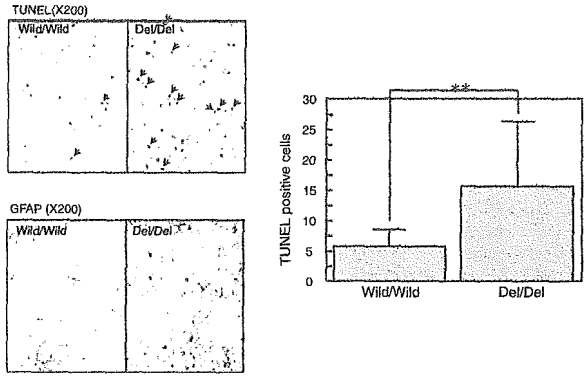

Fig. 5 Terminal transferase biotinylated-UTP nick end-labeling (TUNEL) stain of the striatum of 72–84-week-old wild-type and *CHAC* mutant mice. TUNEL stain, staining the apoptotic cells; many more TUNEL-positive cells were detected in *CHAC* mutant compared with wild-type striatum. Gliosis was found as a marked increase of glial fibrillary acidic protein (GFAP)-immunopositive cells. In TUNEL stain, TUNEL-positive cells in the striatum were counted in every five fields (200 ×) of three wild-type and three *CHAC* mutant mice. The means ± SD of TUNEL-positive cells are shown. There was a significant difference (**$p < 0.001$).

Histopathological and immunohistochemical study of the brain and muscle

In the striatum, remarkable gliosis was detected by anti-glial fibrillary acidic protein antibody in some mutant mice. Apoptosis to a marked degree was detected in the striatum of the mutant mice by the TUNEL staining method. The numbers of TUNEL-positive cells in the striatum of mutant mice were significantly greater than those of wild-type mice (Fig. 5). In some mutant mice, gliosis was marked in the pars reticulata of the substantia nigra (data not shown). These findings were quite similar to the findings in the brain of human CHAC autopsied cases (Hardie *et al.* 1991; Rinne *et al.* 1994).

Discussion

We identified the mouse *CHAC* cDNA sequence and confirmed that the exon–intron organization of the mouse *CHAC* gene is exactly the same as that of the human gene. We then generated and characterized a targeted CHAC model mouse in which exons 60 and 61 of the *CHAC* gene are deleted. The above deletion including exons 60 and 61, Ehime deletion mutation, is found in human Japanese patients suffering from CHAC (Ueno *et al.* 2001). The deletion is present in the coding region of the cDNA resulting in a frame shift and the production of a truncated protein. The *CHAC* mutant mice are viable and reproduce successfully but, after becoming old, they display disturbances in motor function and blood morphological changes which are similar to the features of adult onset and gradual progress seen in human CHAC (Rampoldi *et al.* 2002).

In the present study, the ratio of striatum : whole brain was significantly smaller in the mutant than wild-type mice, which means the selective atrophy of the striatum. Immunohistochemical study of targeted CHAC model mice showed significantly more apoptotic cells in the striatum. The number of TUNEL-positive cells in the striatum of mutant mice was much greater than that of glial fibrillary acidic protein-positive astroglial cells (Fig. 5), which means that most of the TUNEL-positive cells should be neurons. However, intact neuronal cells still seemed to be much more numerous than TUNEL-positive apoptotic cells in mutant mice striatum (Fig. 5), which may explain the discrepancy of normal striatal GABA level in mutant mice (Table 1) despite a marked increase in TUNEL-positive cells. Biochemical analysis showed a significant decrease in HVA concentration in the portion including midbrain of the mutant mice. The main neuropathological finding of CHAC is the degeneration of striatum (Hardie *et al.* 1991). Detailed neuropathological and biochemical findings of human CHAC have only been reported in several autopsy cases. de Yebenes *et al.* (1988) studied neurochemical findings in two autopsy cases of recessive-type neuroacanthocytosis. They determined the levels of monoamines and their metabolites, GABA and

substance P in brain areas. They found depletion of dopamine and its metabolite HVA in the striatum and a marked reduction of HVA in the substantia nigra. Rinne *et al.* (1994) reported the degeneration of the substantia nigra as well as the striatum in some cases of CHAC. The pathological findings in the mutant mouse in the present study coincide well with those in human CHAC mentioned above.

The symptoms and clinical findings of CHAC resemble those of Huntington's disease (Rampoldi *et al.* 2002). Various kinds of model Huntington's disease mice have been produced. Reynolds *et al.* (1999) examined several brain regions of R6/2 transgenic mice, which carry human huntingtin exon 1 including the expanded polyglutamine tract, measuring GABA, glutamate and monoamine neurotransmitters by HPLC. They found that 5-hydroxytryptamine in all brain areas and dopamine in the striatum of older mice decreased, which is related to basal ganglia dysfunction linked to involuntary movements. In this study, *CHAC* mutant mice showed a significant decrease of HVA in the portion including midbrain, thalamus and hypothalamus. Dopamine also decreased but was not significant. Immunohistochemical findings revealed gliosis in the striatum and substantia nigra where degeneration is also found in Huntington's disease (Reddy *et al.* 1998; Lin *et al.* 2001). These results indicate that the dopamine system innervating basal ganglia in *CHAC* mutant mice was impaired. *CHAC* mutant mice did not show any weight loss and showed longevity. However, the results of behavioral analysis indicated the existence of motor dysfunction in old age although the characteristics of motor dysfunction in the mutant mice were distinct from human symptoms seen in CHAC despite the coincidence of the neuropathology. Human patients with CHAC present chorea as the major motor symptom but the model mice showed gait disturbance and early fall from the rotarod without any involuntary movements. Similar discrepancies have been reported repeatedly in many kinds of Huntington's disease model transgenic or knock-in mice (Menalled *et al.* 2002). Phylogenetical differences in the development of basal ganglia may be one of the reasons for the discrepancies in motor function.

Almost complete reproduction of the above human neuropathology in the *CHAC* mutant mouse, together with the phenotypes of motor disturbances and hematological abnormalities, make the model mouse ideal for understanding the molecular pathogenesis of CHAC.

Acknowledgements

The authors thank Ms Tanabe and Mr Kodama for their technical assistance and Dr Izumo for valuable discussion. This work was supported in part by a Grant-in-Aid for Research from the Ministry of Education, Culture, Sports, Science and Technology, Japan.

References

Becker P. S. and Lux S. E. (1995) Hereditary spherocytosis and hereditary elliptocytosis, in *The Metabolic Basis of Inherited Disease* (Scriver C. R. and Beaudet A. L., eds), pp. 3513–3560. McGraw-Hill, New York.

Brickner J. H. and Fuller R. S. (1997) SOI1 encodes a novel conserved protein that promotes TGN-endosomal cycling of Kex2p and other membrane proteins by modulating the function of two TGN localization signals. *J. Cell Biol.* **139**, 23–36.

Brin M. F. (1993) Acanthocytosis, in *Handbook of Clinical Neurology* (Goetz C. G., Tanner C. M. and Aminoff M. J., eds), Vol. 63, pp. 271–299. Elsevier Science B.V., Amsterdam.

Carter R. J., Lione L. A., Humby T. *et al.* (1999) Characterization of progressive motor deficits in mice transgenic for the human Huntington's disease mutation. *J. Neurosci.* **19**, 3248–3257.

Hardie R. J., Pullon H. W., Harding A. E. *et al.* (1991) Neuroacanthocytosis. A clinical, haematological and pathological study of 19 cases. *Brain* **114**, 13–49.

Kageyama Y., Kodama Y., Tadano M., Yamamoto S. and Ichikawa K. (2000) A case of chorea-acanthocytosis with dilated cardiomyopathy and myopathy. *Rinsho Shinkeigaku* **40**, 816–820.

Koera K., Nakamura K., Nakao K., Miyoshi J., Toyoshima K., Hatta T., Otani H., Aiba A. and Katsuki M. (1997) K-Ras is essential for the development of the mouse embryo. *Oncogene* **15**, 1151–1159.

Lin C. H., Tallaksen-Greene S., Chien W. M., Cearley J. A., Jackson W. S., Crouse A. B., Ren S., Li X. J., Albin R. L. and Detloff P. J. (2001) Neurological abnormalities in a knock-in mouse model of Huntington's disease. *Hum. Mol. Genet.* **10**, 137–144.

McIlwain H. and Voaden M. J. (1975) Dissection of the brain to regional blocks, in *Practical Neurochemistry* (McIlwain H., ed.), pp. 284–289. Churchill Livingstone, New York.

Menalled L. B., Sison J. D., Wu Y. *et al.* (2002) Early Motor dysfunction and striosomal distribution of huntingtin Micro aggregates in Huntington's disease Knock-in Mice. *J. Neursci.* **22**, 8266–8276.

Palek J. (1991) Red cell membrane disorders, in *Hematology: Basic Principles and Practice* (Hoffman R., Benz E. J. Jr, Furie B., Shattil S., Cohen H., eds), pp. 472–504. Churchill Livingstone, New York.

Rampoldi L., Dobson-Stone C., Rubio J. P. *et al.* (2001) A conserved sorting-associated protein is mutant in chorea-acanthocytosis. *Nat. Genet.* **28**, 119–120.

Rampoldi L., Danek A. and Monaco A. P. (2002) Clinical features and molecular bases of neuroacanthocytosis. *J. Mol. Med.* **80**, 475–491.

Reddy P. H., Williams M., Charles V., Garrett L., Pike-Buchanan L., Whetsell W. O. Jr, Miller G. and Tagle D. A. (1998) Behavioural abnormalities and selective neuronal loss in HD transgenic mice expressing mutated full-length HD cDNA. *Nat. Genet.* **20**, 198–202.

Reynolds G. P. and Pearson S. J. (1987) Decreased glutamic acid and increased 5-hydroxytryptamine in Huntington's disease brain. *Neurosci. Lett.* **78**, 233–238.

Reynolds G. P., Dalton C. F., Tillery C. L., Mangiarini L., Davies S. W. and Bates G. P. (1999) Brain neurotransmitter deficits in mice transgenic for the Huntington's disease mutation. *J. Neurochem.* **72**, 1773–1776.

Rinne J. O., Daniel S. E., Scaravilli F., Harding A. E. and Marsden C. D. (1994) Nigral degeneration in neuroacanthocytosis. *Neurology* **44**, 1629–1632.

Try K. (1980) Lineation of the osmotic fragility curve of erythrocytes. *Scand. J. Haematol.* **24**, 157–161.

Ueno S., Maruki Y., Nakamura M., Tomemori Y., Kamae K., Tanabe H., Yamashita Y., Matsuda S., Kaneko S. and Sano A. (2001) The gene

encoding a newly discovered protein, chorein, is mutated in chorea-acanthocytosis. *Nat. Genet.* **28**, 121–122.

Yagi T., Nada S., Watanabe N., Tamemoto H., Kohmura N., Ikawa Y. and Aizawa S. (1993) A novel negative selection for homologous recombinants using diphtheria toxin A fragment gene. *Anal. Biochem.* **214**, 77–86.

de Yebenes J. G., Brin M. F., Mena M. A. *et al.* (1988) Neurochemical findings in neuroacanthocytosis. *Mov. Disord.* **3**, 300–312.

ヒト正常型c-Ha-ras遺伝子トランスジェニックラットの乳腺発がん高感受性の機序解析－化学発がんと自然発がんの比較－

濱口 哲也・松岡 洋一郎・川口 博明・高須賀 信夫
深町 勝巳・吉田 浩己・津田 洋幸

乳癌基礎研究会

ヒト正常型c-Ha-ras遺伝子トランスジェニックラットの乳腺発がん高感受性の機序解析－化学発がんと自然発がんの比較－

濱口 哲也[1),2)]・松岡 洋一郎[1)]・川口 博明[3)]・高須賀 信夫[1)]
深町 勝巳[1),2)]・吉田 浩己[3)]・津田 洋幸[1),4)]

[1)]国立がんセンター研究所 化学療法部・[2)]「がん克服新10か年戦略」事業に基づく財団法人がん研究振興財団のリサーチ・レジデント
[3)]鹿児島大学大学院医歯学総合研究科 腫瘍病態学分野・[4)]名古屋市立大学大学院医学研究科 分子毒性学分野

要 旨

当研究部で樹立したヒト正常型c-Ha-rasトランスジェニックラット（Tg）は乳腺発がん高感受性形質である。我々はこれまで、性成熟期Tg乳腺では、化学発がん物質の標的と考えられているTerminal Endbud（TEB）の過剰増生と増殖シグナルの遷延が認められ、その原因としてRas-MAPキナーゼ情報伝達系の持続的活性化が寄与していることを報告してきた。今回は、自然発がんと化学発がんにおけるTg乳腺がんの発生母地の異同を検討した。7、10、15、20週齢TgへDMBA投与により乳腺発がんを誘発すると週齢の増加とともに腫瘍発生率の低下傾向を認めた。1個体あたりの腫瘍数は7週齢時投与群（n＝8）11.3±7.1、10週齢時投与群（n＝10）7.5±4.8、15週齢時投与群（n＝10）4.6±5.3、20週齢時投与群（n＝10）3.6±3.3と15週齢、20週齢時投与群で有意に減少した。また、MNU投与後5日目のTEBですでに導入ras遺伝子（コドン12）の変異がRFLP法により検出された。すなわち、Tg乳腺でもTEBが化学発がん物質の主要標的組織と考えられる。一方、自然発生腫瘍の観察では35週齢Tgのほぼ100％に前がん病変である小葉過形成が、40％には腺がんが発生した。また、Ha-ras、サイクリンD1、サイクリンD2遺伝子の発現が加齢に伴い再上昇していた。RFLP法により75％の過形成性結節で導入Ha-ras遺伝子（コドン12）の点変異が検出されたが、25％の結節並びに他の臓器には変異は検出されなかった。すなわち、Tg乳腺の自然発生腫瘍は腺房を発生母地とし、Ha-ras遺伝子の発現上昇のみで前がん病変が形成され得ることを示している。

はじめに

未経産雌ラットへのN-methyl-N-nitrosourea（MNU）や7,12-dimethylbenz [a] anthracene（DMBA）投与による乳腺発がん誘導はヒト乳がんの実験モデルとして広く用いられている[1)]。思春期乳腺では卵巣ホルモン、下垂体ホルモンや他の成長因子がterminal endbud（TEB）の形成を促進する[2,3)]。RussoらはDMBAによる発がんモデルを用いてTEBから乳がんが発生するとの仮説を提唱している[1),2)]。TEBが発がん高感受性である原因として、この組織が高い増殖能を有する上皮細胞から成ることによると思われる。TEBの上皮細胞の細胞周期は10時間で、DMBAのDNA付加体を高頻度に生じる[2)]。

肺がん、大腸がん、膵臓がんなど一般的なヒトがんはしばしば活性化rasがん遺伝子を有する。ラット乳腺腫瘍、特にMNUにより誘発された腫瘍においてもしばしば活性化H-rasがん遺伝子が検出される[4)-6)]。ras遺伝子の活性化は乳がん発生以前に生ずるが[7)]、がん発生以前の乳腺上皮細胞にras遺伝子変異が起こる直接証拠は呈示されていない。

我々はヒト正常型c-Ha-ras遺伝子トランスジェニック（Tg）ラットを樹立し、乳腺、膀胱、皮膚が化学発がん物質に高感受性であることを

連絡先：関西医科大学 第二病理
〒570-8506 大阪府守口市文園町10-15
Tel: 06-6993-9432 Fax: 06-6992-5023
E-mail: matsuoyo@takii.kmu.ac.jp

報告してきた[6),8),9)]。すべてのラットにおいてMNU投与後20日以内に乳腺前がん病変が発生し[10)]、種々の発がん物質投与により8週以内に乳がんが発生する[6),11)]。興味深いことに、これらのがん組織では内在性ラットras遺伝子に比較してヒトras遺伝子に優先的に変異が認められる[6)]。また、導入ras遺伝子はラット第5染色体のq24-q31.1領域に存在し、近傍には既知のがん遺伝子やがん抑制遺伝子は同定されていない[12)]。

我々はここにTgラット乳腺ではTEBが化学発がん物質の主要標的組織であることを示す。これに対しTgラットの自然発生腫瘍は正常型c-Ha-ras遺伝子の高発現を伴う小葉過形成から発生し、導入ras遺伝子の変異を必ずしも必要としないと予想される。我々の結果は正常型c-Ha-ras遺伝子の高発現が小葉過形成の原因となることを示唆している。

結 果

TgラットにおけるTEB数と化学発がん物質による腫瘍発生の関係

当研究部で樹立したヒト正常型c-Ha-ras遺伝子Tgラットの乳腺発がん高感受性の要因として、Ras-MAPキナーゼ情報伝達系の活性化による細胞増殖亢進、さらにTEBの過剰増生が寄与しているらしいことを報告してきた[13),14)]。Tg、non-Tgラットともに7週齢時、10週齢時、15週齢時、20週齢時にDMBAを投与する各4群とした。Tgラットは投与後8週、non-Tgラットは投与後20週で屠殺し、その間触診にて腫瘍を観察した。non-Tgラットでは7週齢時にDMBAを投与すると58.4％の個体に触知可能な乳腺腫瘍が発生し、投与時期を遅らせるに従い腫瘍発生率には減少する傾向を認めた（図1A）。解剖時での腫瘍発生率と乳腺腫瘍の平均重量には4群間で有意差は認められなかったが、1個体あたりの腺がん発生数は7週齢時投与群と比較して15週齢、20週齢時投与群で有意に減少した（図1C、表1）。一方Tgラットでは、投与後8週で7週齢時投与群の全個体に触知可能な腫瘍が発生し、10週齢、15週齢、20週齢時に投与した群でも70％の個体で触知可能な腫瘍が発生した（図1B）。解剖時での腫瘍発生率と乳腺腫瘍の平均重量には4群間で差はなかった（表2）。しかし、1個体あたりの腺がん発生数には7週齢時投与群と比較して15週齢時投与群、20週齢時投与群で有意な減少が認められた（図1D、表2）。我々の結果は、TEBが化学発がん物質の主要標的組織であるとの仮説に一致する。

乳管の早期がん病変はTEBの近傍に発生する

TgラットではMNU投与後20日で乳管に増殖性病変が発生する[10)]。病変のほとんどはTEBの乳頭側近傍に認められ、MNU投与時にはTEBであった部位から生じたものと考えられる。組織学的診断では、これらの病変は異型過形成もしくは腺がんである[10)]。

TEBは化学発がん物質の標的組織である

Tgラットでは内在性ラットras遺伝子と比較してヒトc-Ha-ras遺伝子に高頻度の変異が検出されるため、導入ras遺伝子を変異検出のためのプローブとして用いた[6)]。MNU投与後5、10、15日目に屠殺したTgラットのTEBよりDNAを単離し、ras遺伝子の変異の有無をrestriction fragment length polymorphism (RFLP) 解析法により検討した。この結果、腺がんの発生は稀である投与後5－15日目ですでにras遺伝子（コドン12）に変異が検出された（図2）。尚、コドン61には変異は検出されなかった。以上の結果からTEBはTgラット乳腺における化学発がん物質の主要標的組織の1つであると考えられる。

Tgラット乳腺の自然発生腫瘍と小葉過形成

未経産Tgラットを経過観察すると、11週齢で初めて乳腺に自然発生腫瘍が触知され(1/36)、その後加齢とともに腫瘍発生率は増加し、40週齢で52.8％（19/36）に達した（図3）。35週齢時に触知された全ての腫瘍は組織学的には腺がんであった。未経産TgラットではTEBだけではなく乳管上皮細胞においても増殖活性が上昇していた。70日齢での乳管上皮

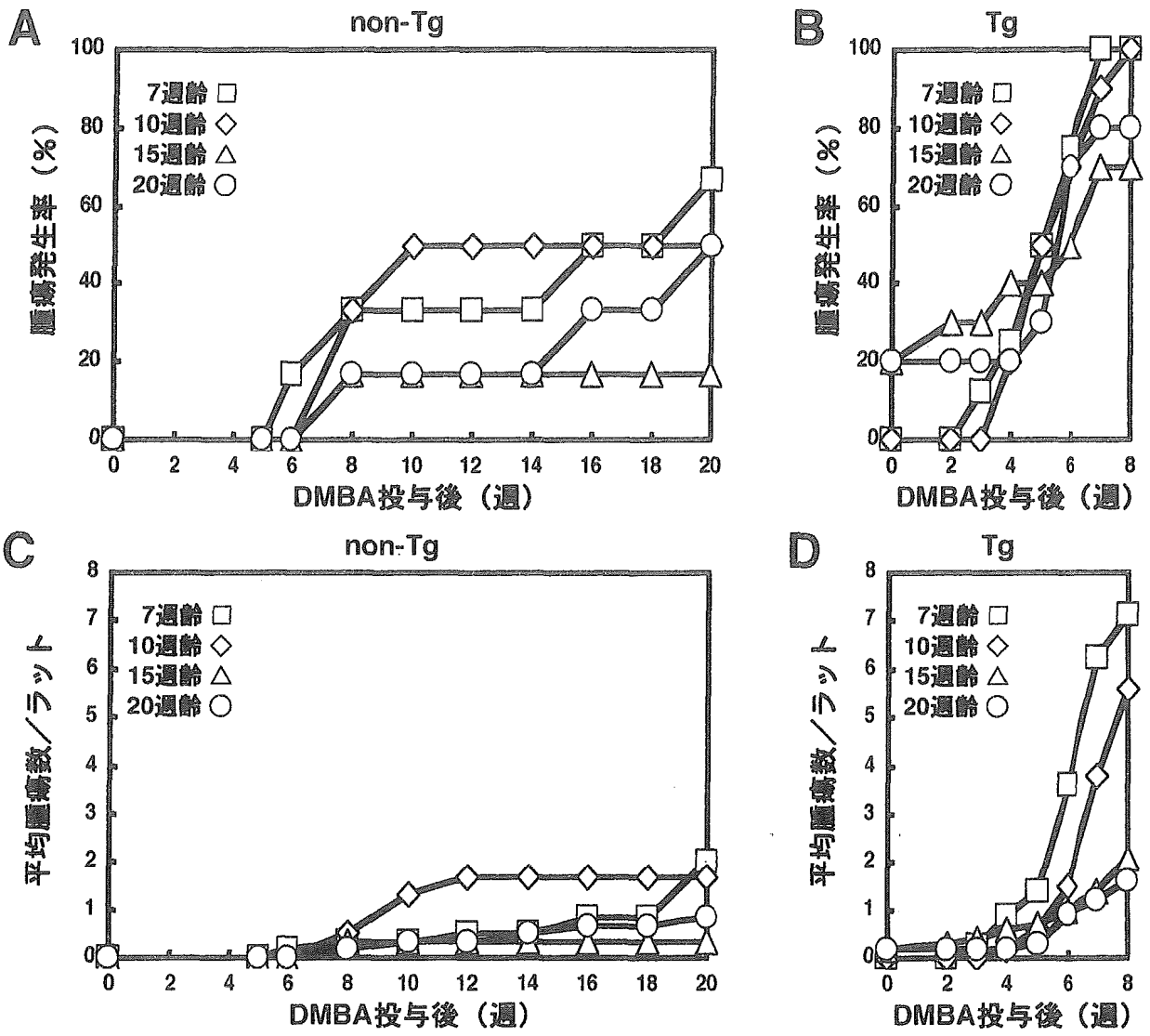

図1　DMBA投与時週齢と乳腺腫瘍発生頻度、発生数との関係

ラットは7週齢（□）、10週齢（◇）、15週齢（△）、20週齢（○）にDMBA胃内単投与した。（A、B）DMBA投与後の腫瘍発生率、（C、D）1個体あたりの平均発生腫瘍数。

表1　DMBA投与non-Tgラットの屠殺時の腫瘍発生率と腫瘍重量

DMBA投与週齢（週）	個体数	異型過形成		腺がん		計		腫瘍重量 (mean±SD)
		1個体あたりの腫瘍数		1個体あたりの腫瘍数		1個体あたりの腫瘍数		
		腫瘍発生率(%)	(mean±SD)	腫瘍発生率(%)	(mean±SD)	腫瘍発生率(%)	(mean±SD)	
7	6	0 (0)	0	5 (83.3)	4.7±4.0	5 (83.3)	4.7±4.0	3.33±5.58
10	6	1 (16.7)	0.3±0.8	4 (66.7)	2.0±2.1	3 (66.7)	2.3±2.6	3.26±6.83
15	6	1 (16.7)	0.2±0.4	1 (16.7)	0.2±0.4[a]	2 (33.3)	0.3±0.5[a]	0.01±0.01
20	6	0 (0)	0	3 (50)	0.8±1.2[b]	3 (50)	0.8±1.2[b]	1.03±1.55

[a]$p<0.01$ （7週齢投与群と比較して）
[b]$p<0.05$ （7週齢投与群と比較して）

表2　DMBA投与Tgラットの屠殺時の腫瘍発生率と腫瘍重量

DMBA投与週齢(週)	個体数	異型過形成 1個体あたりの腫瘍数 腫瘍発生率(%)	異型過形成 1個体あたりの腫瘍数 (mean±SD)	腺がん 1個体あたりの腫瘍数 腫瘍発生率(%)	腺がん 1個体あたりの腫瘍数 (mean±SD)	計 1個体あたりの腫瘍数 腫瘍発生率(%)	計 1個体あたりの腫瘍数 (mean±SD)	腫瘍重量 (mean±SD)
7	8	0 (0)	0	8 (80)	11.3±7.1	8 (100)	11.3±7.1	6.70±9.03
10	10	0 (0)	0	10 100)	7.5±4.8	10 (100)	7.5±4.8	2.92±2.38
15	10	0 (0)	0	8 (80)	4.6±5.3[a]	8 (80)	4.6±5.3[a]	4.73±6.42
20	10	0 (0)	0	8 (80)	3.6±3.3[b]	8 (80)	3.6±3.3[b]	5.69±7.60

[a]p<0.05 （7週齢投与群と比較して）
[b]p<0.01 （7週齢投与群と比較して）

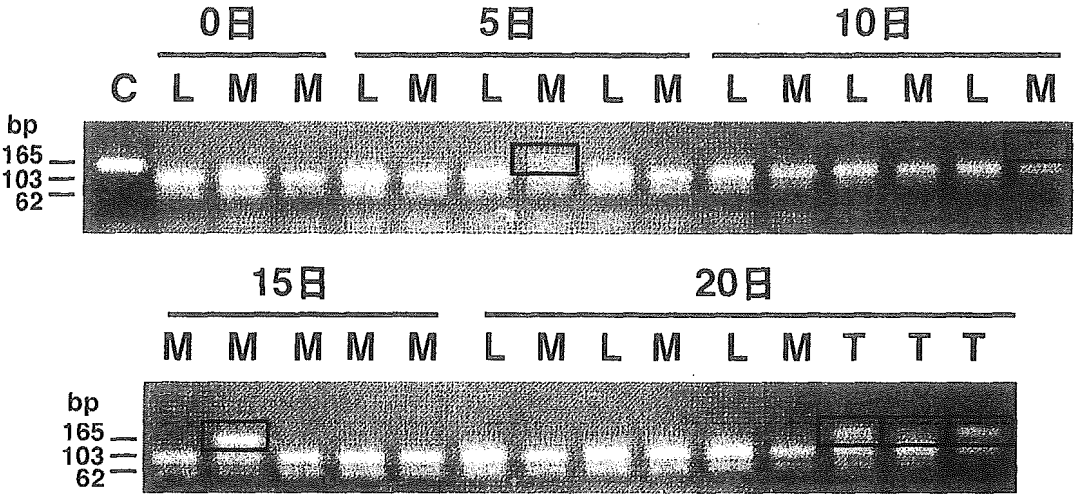

図2　MNU投与後早期におけるTEBのras遺伝子変異
MNU投与後20日目までのTEBにおけるヒトras遺伝子（コドン12）変異をRFLP法にて解析した結果を示す。Tgラット各個体当り3－5個のTEBからDNAを抽出した。C、コドン12を有する対照cDNA；L、TEB DNAを抽出したラットの肝臓DNA；M、TEBから単離したDNA；T、3匹のTgラットに発生した乳腺腫瘍のDNA；□、変異ras遺伝子を示す。

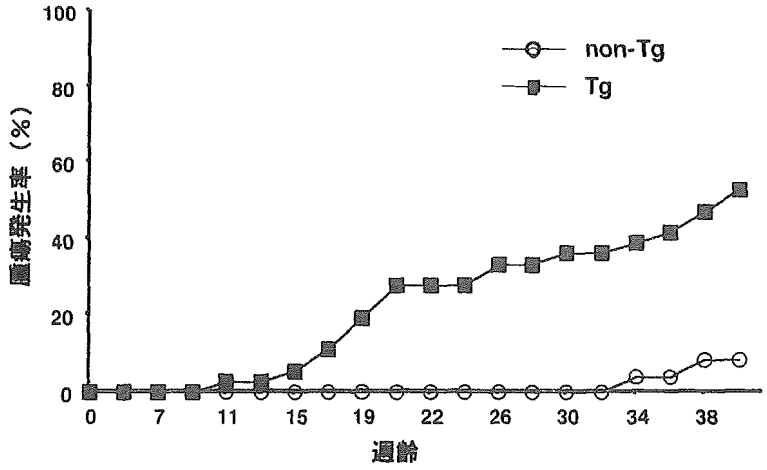

図3　non-Tg、Tgラットに自然発生する乳腺腫瘍の発生頻度
観察個体数はnon-Tgラット24匹、Tgラット36匹で、触診にて腫瘍の有無を観察した。

のproliferating cell nuclear antigen (PCNA) 陽染核数はTgラット (15.2±3.1%、n=3) でnon-Tgラット (6.6±1.1%、n=3) に比較して有意 ($p<0.01$) に多かった。少数の小葉と細い乳管から成る42週齢non-Tgラット乳腺 (図4A, D) と対照的に、35週齢Tgラット乳腺のほとんどは妊娠乳腺様で、終末乳管と小葉の増加、び慢性の小葉過形成結節を認めた (図4B, E)。時折過形成結節の上皮細胞には異型性が認められた (図4C, F)。

Tgラット乳腺におけるras遺伝子、サイクリンD遺伝子ファミリーの再上昇と小葉過形成の発生

10－35週齢Tgラット乳腺のヒトおよびラットc-Ha-ras遺伝子の発現量を解析した (図5A)。対象乳腺には数個から全ての小葉に細胞異型を伴うあるいは伴わない過形成が認められた (図4)。ras (ヒトおよびラット) 遺伝子の発現量は17週齢で再上昇し、35週齢で10週齢に比べ3.6倍の発現上昇を認めた。ras遺伝子の再上昇と平行してサイクリンD1、D2遺伝子のmRNA量も17週齢、35週齢で明らかな上昇を認めた。サイクリンD3遺伝子の発現は35週齢で上昇を認めた。

小葉過形成は前がん病変と考えられていることから、過形成結節のヒトras遺伝子の変異を検証した。5匹のラットから得られた8個の結節につき検討した結果75% (6/8) の検体に変異 (コドン12) が検出された (図5B)。これは小葉過形成の前がん病変としての性質を支持する結果である。

しかし、2つの検体では変異は検出されなかった (図5B、レーン5、12)。変異が検出された検体においても野生型ras由来のバンド(103、62bp) が常に変異ras由来のバンド (165bp) より優勢であることから、ras変異を有する細胞は少数と考えられた。尚、コドン61には変異は検出されなかった。以上の結果より小葉過形成結節における過形成性変化はras遺伝子の過剰発現によるもので、ras遺伝子の変異によるものではないと考えられる。

考 察

ヒトの腫瘍はしばしば点変異により活性化されたras蛋白質を発現している－全腫瘍の約20%にH-、K-、N-ras遺伝子のいずれかに点変異が認められる。多くの例で、このような変化はすでに前がん病変で起きていることから、ras遺伝子変異は発がんの初期段階に関わっていると考えられる。c-Ha-ras Tgラットはnon-Tgラットに比べTEB数が多く、発がん物質の投与後早期 (5日目) に正常形態のTEBで導入遺伝子の変異が検出された (図2)。これは化学発がん物質によるras遺伝子変異がTEBで起きていることを示す最初の直接証拠である。non-Tgラット (図1C、表1) 同様Tgラットにおいてもteb数と1個体あたりの腫瘍数に相関性が認められ (図1D、表2)、この事からもTEBが化学発がん物質の主要標的組織であると考えられる。

TEB数だけではなく乳腺の増殖状態も発がん感受性を規定する因子として重要である。TgラットのTEB数は91日 (13週) 齢でnon-Tgラットと同じとなる[12]。ところが、15週齢および、20週齢でDMBAを投与されたTgラットの投与後8週における1個体当たりの腫瘍数はnon-Tgに比較して6～9倍多い (図1C, D)。TgラットのTEBでは細胞増殖活性がより高く、腫瘍の増殖速度もきわめて速い[10]。また、性成熟期のTgラット乳腺ではH-ras、c-myc、サイクリンDの発現が上昇している (未発表)。すなわち、Tgラット乳腺の高い増殖活性がTEB数と同等かそれ以上に発がん高感受性の重要因子であると考えられる。

がんは正常上皮細胞から脱分化し、いくつかの段階を経てがん化する。早期のがん化過程を研究することはがんの治療・予防に最適な細胞レベル、分子レベルでの標的を発見することにつながると考えられる。乳腺における前がん病変は小葉過形成と乳管過形成である[15]。最近の研究では多数の遺伝子の機能異常がマウスの乳がんで認められているが、細胞周期調節遺伝子を始めとして遺伝子変異はほとんど検出されていない。小葉過形成結節の移植実験で前がん病

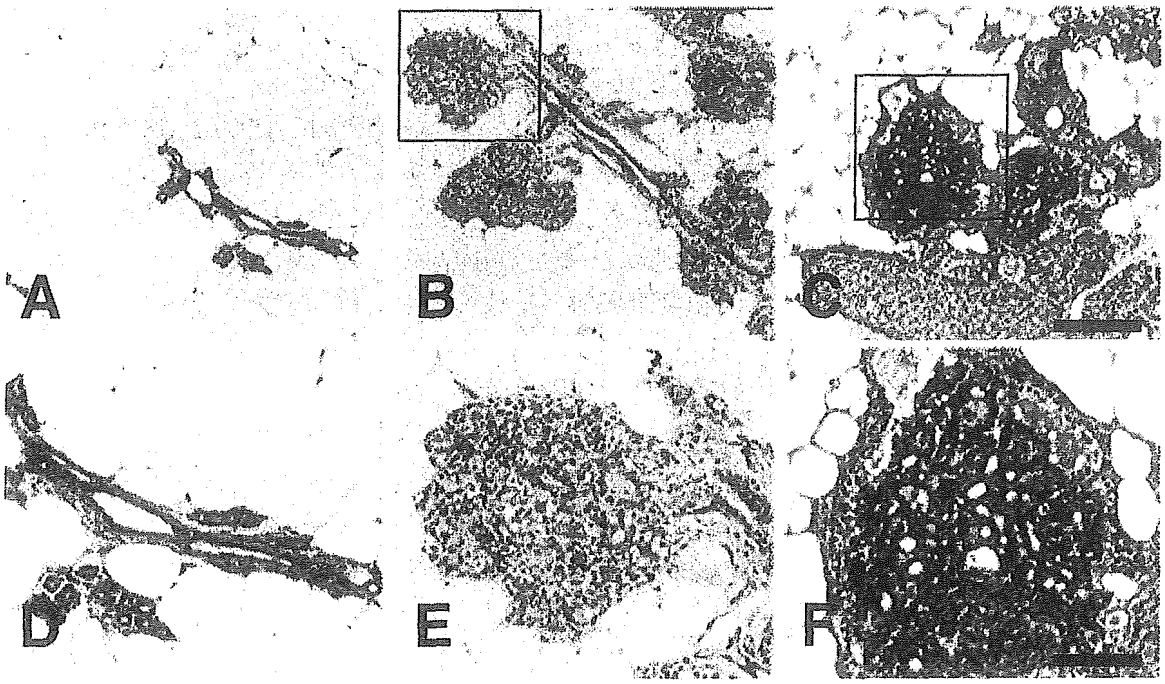

図4　35週齢non-Tg、Tgラット乳腺のHE像
小葉過形成が全てのTgラット乳腺に観察され、細胞異型を伴わないもの（B、E）と伴うもの（C、F）を認めた。D、E、Fはそれぞれ A、B、Cの強拡像。A－Cのスケールは250 μm、D－Fのスケールは100 μm を示す。

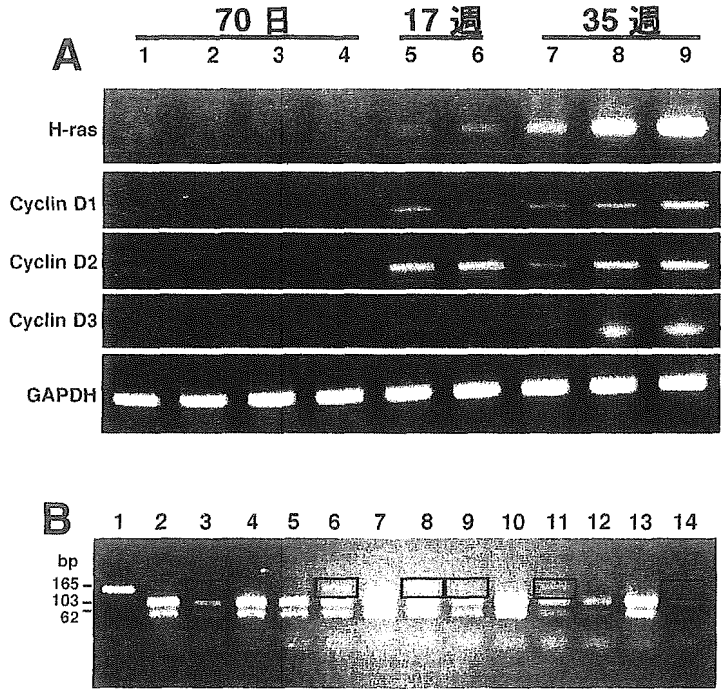

図5　Tg乳腺におけるc-Ha-ras遺伝子発現の再上昇と小葉過形成結節でのras遺伝子変異
(A) RT-PCR法による10週齢、17週齢、35週齢Tgラット乳腺でのヒトおよびラットc-Ha-ras (H-ras) 遺伝子、サイクリンD1、D2、D3遺伝子の発現解析。(B) RFLP法による小葉過形成結節でのヒトras遺伝子（コドン12）変異の解析像。レーン1、コドン12に変異を有する対照cDNA；レーン2、4、7、10、13、Tgラットの肝臓DNA；レーン3、5、6、8、9、11、12、14、小葉過形成結節から単離したDNA。検体はTgラット5匹から採取した。□、変異ras遺伝子のバンドを示す。

変におけるサイクリンB1、D1、Eの発現上昇と$p21^{WAF1}$や$p16^{INK4a}$の発現低下が示されている[15]。サイクリンD1、D2の発現はTgラットの小葉過形成においても上昇している（図5A）。さらに、Tgラットには化学発がん物質投与後15日でもう一つの前がん病変である乳管過形成が発生する[10]。ラットとヒトの乳がんは組織学的、機能的に類似しており、ラット乳がんの生物学的特性を解明することはヒト乳がんの克服に大いに資するものと期待される。

謝　辞

山口愛女史には組織染色に御協力をいただきましたことを深謝いたします。

文　献

1) Russo, J. et al: Susceptibility of the mammary gland to carcinogenesis: I Differentiation of the mammary gland as determinant of tumor incidence and type of lesion, Am J Pathol 96: 721-36, 1979
2) Russo, J. et al: Biological and molecular bases of mammary carcinogenesis, Lab Invest 57: 112-37, 1987
3) Humphreys RC: Programmed cell death in the terminal endbud. J Mammary Gland Biol, Neoplasia 4: 213-20, 1999
4) Sukumar, S. et al: Induction of mammary carcinomas in rats by nitroso-methylurea involves malignant activation of H-ras-1 locus by single point mutations, Nature 306: 658-61, 1983
5) Leon, J. et al: H-ras activation in benign and self-regressing skin tumors (keratoacanthomas) in both humans and an animal model system, Mol Cell Biol 8: 786-93, 1988
6) Asamoto, M. et al: Transgenic rats carrying human c-Ha-ras proto-oncogenes are highly susceptible to N-methyl-N-nitrosourea mammary carcinogenesis, Carcinogenesis 21: 243-9, 2000
7) Kumar, R. et al: Activation of ras oncogenes preceding the onset of neoplasia, Science 248: 1101-4, 1990
8) Ota, T. et al: Transgenic rats carrying copies of the human c-Ha-ras proto-oncogene exhibit enhanced susceptibility to N-butyl-N-(4-hydroxybutyl) nitrosamine bladder carcinogenesis. Carcinogenesis 21: 1391-6, 2000
9) Tsuda, H.: High susceptibility of transgenic rats carrying the human c-Ha-ras proto-oncogene to chemically-induced mammary carcinogenesis, Mutat Res 477: 173-82, 2001
10) Matsuoka, Y. et al: Rapid emergence of mammary preneoplastic and malignant lesions in human c-Ha-ras proto-oncogene transgenic rats: possible application for screening of chemopreventive agents, Toxicol Pathol 31(6): 632-637, 2003
11) Han, BS. et al: Inhibitory effects of 17beta-estradiol and 4-n-octylphenol on 7,12-dimethylbenz[a] anthracene-induced mammary tumor development in human c-Ha-ras proto-oncogene transgenic rats, Carcinogenesis 23: 1209-15, 2002
12) Hamaguchi, H. et al: Terminal endbuds and acini as the respective major targets for chemical and sporadic carcinogenesis in the mammary glands of human c-Ha-ras protooncogene transgenic rats, Breast Cancer Res Treat: in press, 2004
13) 松岡洋一郎・他: ヒト正常型c-Ha-ras遺伝子トランスジェニックラットの乳腺発がん高感受性の機序解析，乳癌基礎研究 11: 33-36, 2002
14) 濱口哲也・他：ヒト正常型c-Ha-ras遺伝子トランスジェニックラットの乳腺発がん高感受性の機序解析—第2報—，乳癌基礎研究 12: 45-50, 2003
15) Medina, D.: Biological and molecular characteristics of the premalignant mouse mammary gland, Biochim Biophys Acta 1603: 1-9, 2002

Breast Cancer Research and Treatment **83:** 43–56, 2004.

Report

Terminal endbuds and acini as the respective major targets for chemical and sporadic carcinogenesis in the mammary glands of human c-Ha-ras protooncogene transgenic rats

Tetsuya Hamaguchi[1,4], Yoichiro Matsuoka[1], Hiroaki Kawaguchi[3], Katsumi Fukamachi[1], Nobuo Takasuka[1], Shinobu Ueda[1], Kimiko Shimizu[2], Misao Ohki[2], Masato Kusunoki[4], Teruyo Sakakura[5], Hiroki Yoshida[3], and Hiroyuki Tsuda[1,6]

[1]*Experimental Pathology and Chemotherapy Division,* [2]*Cancer Genomics Division, National Cancer Center Research Institute, Tsukiji, Chuo-ku, Tokyo;* [3]*First Department of Pathology, Faculty of Medicine, Kagoshima University, Sakuragaoka, Kagoshima;* [4]*Second Department of Surgery,* [5]*First Department of Pathology, Mie University School of Medicine, Edobashi, Tsu, Mie, Japan;* [6]*Present address: Department of Molecular Toxicology, Nagoya City University Graduate School of Medical Sciences, Mizuho-cho, Mizuho-ku, Nagoya, Japan*

Key words: cyclin D, mammary carcinoma, mitogen-activated protein kinase, ras, terminal endbud, transgenic rat

Summary

A rat strain carrying the human c-Ha-ras protooncogene, established by our laboratory, is highly susceptible to mammary chemical carcinogens. The transgenic rats exhibit increased number of terminal endbuds (TEBs) at the tips of developing ducts in the mammary gland compared to non-transgenic littermates. Confocal microscopy revealed the level of active mitogen-activated protein kinase to be elevated in these TEBs, and a close correlation between their numbers and tumorigenic response initiated by 7,12-dimethylbenz[a]anthracene was confirmed. Single injections of *N*-methyl-*N*-nitrosourea into the transgenic rats caused mutations in codon 12 of human c-Ha-ras transgene in TEBs before tumor development, supporting the conclusion that these structures are the major targets of chemical carcinogens. In contrast, with spontaneous development of lesions, alveolar hyperplasia with elevated expression levels of rat and human c-Ha-ras protooncogenes is the first morphological alteration which becomes apparent. Some but not all hyperplastic alveolar nodules were found to harbor mutations in the transgene. The results indicate that elevated expression of c-Ha-ras protooncogene is sufficient in itself to cause a highly proliferative phenotype of mammary alveoli. Our data suggest that TEBs and acini are the major targets for chemical and sporadic carcinogenesis, respectively, in the mammary glands of human c-Ha-ras protooncogene transgenic rats.

Abbreviations: BrdU: 5-bromo-2′-deoxyuridine; DMBA: 7,12-dimethylbenz(a)anthracene; FISH: fluorescence *in situ* hybridization; MAPK: mitogen-activated protein kinase; MNU: *N*-methyl-*N*-nitrosourea; RFLP: restriction fragment length polymorphism; TEB: terminal endbud; Tg: transgenic

Introduction

Induction of mammary carcinogenesis by administration of either *N*-methyl-*N*-nitrosourea (MNU) or 7,12-dimethylbenz[a]anthracene (DMBA) to virgin female rats is widely used for experimental models of neoplasia in the human breast [1–5]. During the pubertal stage of mammary gland development, ovarian and pituitary hormones and locally acting growth factors stimulate the formation of terminal endbuds (TEBs) [6, 7]. Russo et al. have developed the concept that mammary carcinoma arise from TEBs using the DMBA carcinogenesis model [1, 6]. The susceptibility of TEBs to neoplastic transformation has been attributed to the fact that they are composed of an epithelial population with a large proliferative compartment, the

cells of which cycle every 10 h and actively bind DMBA to DNA [6].

Some common forms of human cancer, including carcinomas of the lung, colon, and pancreas, harbor activated ras oncogenes [8, 9]. Molecular analysis of rat mammary tumors has also revealed the presence of activated H-ras oncogenes, particularly in those tumors induced by the direct-acting carcinogen MNU [10–12]. Although activation of ras oncogenes precedes the onset of mammary neoplasia [13], direct evidence that mutations of ras genes occur in mammary epithelial cells before development of the neoplasia has been lacking.

The ras protooncogenes and oncogenes act on the cell cycle machinery through the mitogen-activated protein kinase (MAPK) pathway [14, 15]. Amplification and/or overexpression of protooncogenes such as H-, K-, and N-ras, and neu/erbB-2/HER-2 are frequent events in mammary malignancies of humans [16, 17] and mice [18]. Indeed, breast cancers frequently contain an increased proportion of cells featuring MAPK activation [19, 20]. Moreover, expression of ras oncogenes can cause mammary carcinomas to develop in mice and rats [21–23]. However, the roles of ras protooncogenes during normal development as well as pathological processes of the mammary glands have not been well studied. Since ras not only promotes cell proliferation but also has anti-apoptotic effects [24–27], mammary glands can be used as an excellent model to investigate possible impact of up-regulation of the Ras-MAPK pathway on development and pathology.

We have generated a rat line carrying the human c-Ha-ras protooncogene and demonstrated that it has increased susceptibility to chemical carcinogens targeting the mammary gland, urinary bladder, and skin [12, 28, 29]. All of the rats develop pre-neoplastic mammary lesions within 20 days after injection of MNU [30] and mammary carcinomas within 8 weeks of treatment with a variety of chemical carcinogens [12, 31]. Interestingly, these carcinomas harbor activating mutations, preferentially in the human transgene [12].

We here present evidence indicating that TEBs are major targets of chemical carcinogens in the mammary glands of c-Ha-ras protooncogene transgenic rats. In contrast, spontaneous lesions in these animals appear to arise from alveolar hyperplasia with high expression levels of rat and human c-Ha-ras protooncogenes. This may occur without mutations of the transgene. Our data suggest a causal relationship between overexpression of c-Ha-ras protooncogene and the induction of alveolar hyperplasia.

Materials and methods

Animals and treatment

Female c-Ha-ras transgenic (Tg) and non-transgenic (non-Tg) rats were bred under SPF conditions by CLEA Japan Inc., Tokyo, Japan. They were housed three per cage in an environmentally controlled animal facility maintained at 22°C and 55% relative humidity with a 12 h light–dark cycle. Tg and non-Tg rats were separated into four groups each (7, 10, 15 and 20 weeks of age) and received an intragastric application of 50 mg/kg body weight of 7,12-dimethylbenz(a)anthracene (DMBA) (Tokyo Chemical Industries, Osaka, Japan) at an appropriate age. Tg and non-Tg rats were killed at 8 and 20 weeks after DMBA treatment, respectively. Tumor incidence was assessed by palpation until euthanasia. The experiments were conducted according to the 'Guidelines for Animal Experiments in National Cancer Center' established by the Committee for Ethics of Animal Experimentation of the National Cancer Center, Japan.

Whole-mount preparation of mammary glands

The abdominal–inguinal glands removed from animals were fixed overnight in 10% neutral buffered formalin, rinsed, and then immersed overnight in alum carmine (Chroma, Münster, Germany). TEBs were counted in the left abdominal gland area. Statistical evaluations were performed with the Student's *t*-test.

Measurement of the phosphoMAPK/MAPK ratio

Immunofluorescence staining was performed as described previously [32, 33]. A confocal microscope FLUOVIEW FV300 (Olympus, Tokyo, Japan) was utilized for phosphoMAPK/MAPK imaging of TEB with Alexa Fluor 488-conjugated goat anti-mouse (20 μg/ml) and Alexa Fluor 568-conjugated goat anti-rabbit (8 μg/ml) IgGs (Molecular Probes, Eugene, OR) as secondary antibodies. At least two TEBs in a rat of similar size were selected and scanned to collect fluorescence information under the same parameter settings using argon (channel 1) and helium-neon lasers (channel 2). Calculations of signal ratios of phosphoMAPK/MAPK for each pixel with maximum ratio setting of 2.0 were performed after subtracting

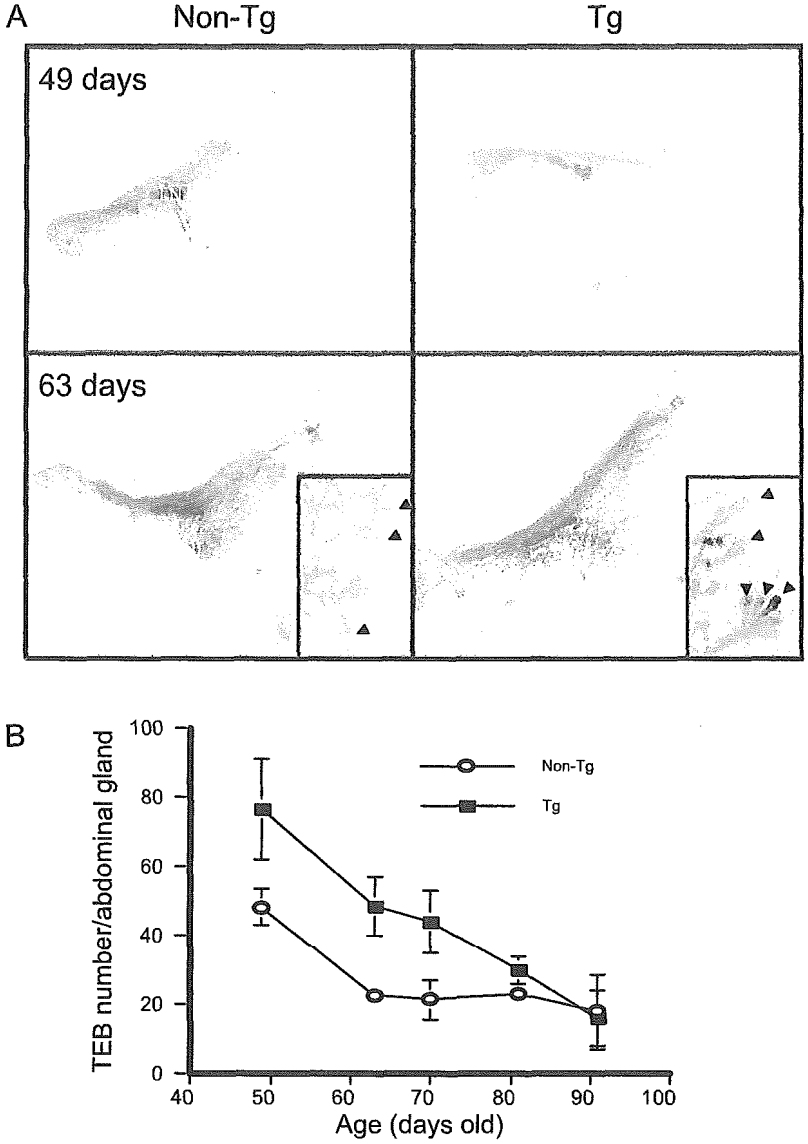

Figure 1. Number of TEBs in non-transgenic and c-Ha-ras transgenic rats during sexual maturation. (A) Representative whole-mount preparations of mammary glands from non-transgenic (non-Tg) and c-Ha-ras transgenic (Tg) virgin rats of 49 or 63 days of age. The photomicrographs of the entire 5th and 6th mammary glands were taken at the same magnification. Inset, higher magnification of TEBs (arrowheads) in 63-day-old rats. LN indicates the lymph node chain of the mammary gland. (B) TEB numbers in the mammary glands of non-transgenic (○) and transgenic (■) rats. Points represent means ± SD of data for at least three rats per time point.

background signals of the surrounding fat tissues. One region of interest covering the entire area of a TEB except the lumen was manually drawn to obtain a mean value for the ratio. The data processing was carried out using software provided by the manufacturer. The final concentrations of the first antibodies were 5 μg/ml for mouse anti-phosphoMAPK and 1 μg/ml for rabbit anti-MAPK (Cell Signaling Technology, Beverly, MA).

Quantitation of cell proliferation

For the analysis of cell proliferation, rats were injected i.p. with 100 mg/kg of 5-bromo-2′-deoxyuridine